

Topological defects lead to energy transfer in active nematics

Daniel J. G. Pearce,¹ Berta Martínez-Prat,^{2,3} Jordi Ignés-Mullol,^{2,3} and Francesc Sagués^{2,3}

¹*Department of Theoretical Physics, University of Geneva, 1205 Geneva, Switzerland*

²*Department of Materials Science and Physical Chemistry, Universitat de Barcelona, Barcelona, 08028, Spain*

³*Institute of Nanoscience and Nanotechnology, IN2UB, Universitat de Barcelona, Barcelona, 08028, Spain*

(Dated: November 28, 2024)

Active nematics are fluids in which the components have nematic symmetry and are driven out of equilibrium due to the microscopic generation of an active stress. When the active stress is high, it drives flows in the nematic and can lead to the proliferation of topological defects, a state we refer to as defect chaos. Using numerical simulations of active nematics, we observe energy transfer between length scales during defect chaos. We demonstrate that this energy transfer is driven by the exchange between variations in the orientation and degree of order in the nematic that predominantly occur during defect creation and annihilation. We then show that the primary features of energy transfer during defect chaos scale with the active length scale. Finally, we identify a second regime that features few defects, but rather bend walls. Similar to topological defects, these bend walls co-localize variations in the orientation with variations in the scalar order parameter leading to energy transfer.

Active matter is the study of systems that are driven out of equilibrium by the generation of stress at the component scale [1–4]. Examples of active materials range from the micrometer scale, for example swimming sperm, through to kilometer scale shoals of fish [5–7]. Active nematics are active fluids in which the components have nematic symmetry [8]. This describes a large class of biosystems including bacterial colonies, the cytoskeleton and epithelial sheets [9–14]. Among the most striking examples of active nematics are those made from reconstituted cytoskeletal components, namely microtubules and kinesins, an experimental system which has been used to demonstrate many properties of active suspensions [15–18]. One of the most prominent features of active nematics is the presence of topological defects, point like discontinuities in the orientation of the nematic components characterized by a half integer winding number [19]. In addition, nematic topological defects have an orientation which effects their motion relative to other defects in the material [20–22]. Topological defects in active nematics also lead to distinct local force patterns, in particular the polar symmetry of +1/2 defects leads them to self propelling [17, 19, 23, 24]. When the active stress is sufficiently high, it generates large flows which destabilize the nematic orientation, leading to defect proliferation and small scale vortices [19], a state we refer to as defect chaos.

Defect chaos is visually similar to classical turbulence, with the distinction that it occurs at low Reynolds number, when classical turbulence is impossible [25]. This similarity has driven a lot of interest in understanding the mechanism behind this phenomenon [19, 26–28]. Giomi showed that the vortices generated during defect chaos have exponentially distributed areas, and identified the scaling parameter as the “active length scale”, the scale at which active and elastic forces balance [19]; these predictions have

been experimentally corroborated [29]. The active length scale, often denoted l_α , is the length scale at which deformations in the nematic director field become unstable due to the flows generated by the active stress, and has been shown to be one of the primary length scales in active nematics, dictating features in the flow field and director field, as well as defect densities and spatial correlations [17, 19]. Giomi also showed that power law scaling was expected in the kinetic energy spectrum in the high wave number range. Simulations by Alert et al. [30] reported additional universal scaling of flow spectra in the range of small wave numbers, with a separating crossover dictated by the active length scale. A more general form of scaling was confirmed in the microtubule/kinesin experimental system taking into account external dissipation [31]. Classical turbulence is also characterized by an energy cascade, in which kinetic energy is transferred between length scales [25]. Alert et al. [30, 32] also addressed this question, considering both elastic and kinetic contributions in the defect free limit. They concluded that within the energy scaling regime there is no energy transfer. Results by Urzay et al. [33] and Carenza et al. [34], considering purely kinetic contributions, are essentially consistent with the lack of energy cascades, although authors in the latter work observed some residual form of energy transfer due to elastic stresses at intermediate length scales.

In this manuscript, we study chaotic flows in active nematics at low Reynolds number. We consider the total energy stored in the system, that being the sum of the kinetic energy and the Landau De-Gennes free energy. We derive the dissipative terms and observe a clear energy transfer between length scales. We demonstrate that this energy transfer is due to an exchange of energy between variations in the orientation of the nematic and its scalar order parameter, a process which happens predominantly during defect annihilation and creation.

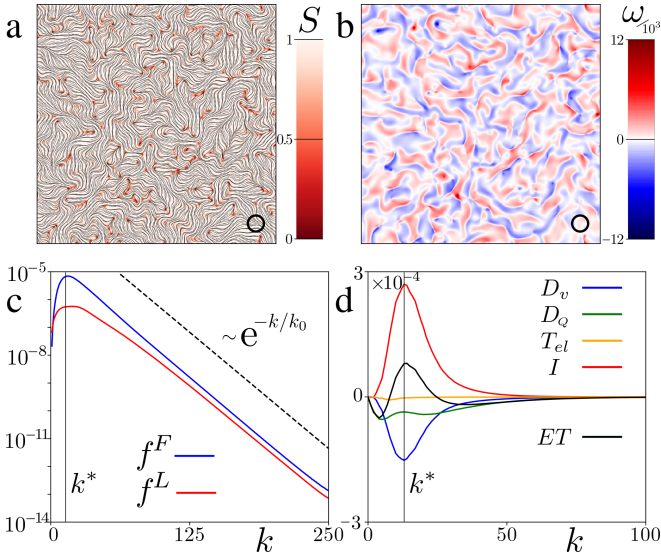


FIG. 1. (a&b) Simulated active nematic showing the director field (lines) and scalar order parameter (color) (a) and vorticity (b). (c) Spectra for the Landau De-Gennes free energy showing the distortion (blue) and scalar order parameter (red) contributions separately. The dashed line shows an exponential distribution with $k_0 \sim 13$; this scale is predominantly governed by the defect core radius, ϵ , rather than the activity, see [35]. (d) Dissipation spectra for a simulated active nematic. This shows a clear energy transfer between length scales given by the black line. The wave number associated with the peak energy injection is identified as $k^* \approx 13$ which also corresponds to the peak in stored elastic energy. The observation that $k^* \approx k_0$ in these results is merely coincidental, see [35]. The length scale associated with this wave number is indicated by the black circle in (a)&(b).

We confirm that in a broad area of parameter space, the active length scale remains the dominant one. Finally, we identify a new regime in the parameter space that is characterized by the presence of bend walls instead of topological defects. This change is associated with a transition from viscous to elastic dissipation.

We study an incompressible two-dimensional active nematic. The nematic texture is described by the \mathbf{Q} tensor which combines the nematic orientation \mathbf{n} and the local degree of nematic order $S \in [0, 1]$ into a single tensorial order parameter $Q_{ij} = S(n_i n_j - \delta_{ij}/2)$. The dynamics of the velocity \mathbf{v} and the nematic tensor \mathbf{Q} are described by the respective equations [36]:

$$\rho D_t \mathbf{v} = \eta \nabla^2 \mathbf{v} + \nabla \cdot (\boldsymbol{\sigma}^p + \boldsymbol{\sigma}^E + \alpha \mathbf{Q}), \quad \nabla \cdot \mathbf{v} = 0, \quad (1)$$

$$D_t \mathbf{Q} = \lambda S \mathbf{u} + \frac{1}{\gamma} \mathbf{H} + \mathbf{Q} \cdot \boldsymbol{\omega} - \boldsymbol{\omega} \cdot \mathbf{Q}. \quad (2)$$

As commonly written, \mathbf{u} and $\boldsymbol{\omega}$ respectively represent the strain rate and vorticity tensors, α is the activity, λ is the dimensionless flow aligning parameter, ρ is a constant density, η is the shear viscosity and γ is the rotational viscosity. The passive stress is given by $\boldsymbol{\sigma}^p = -P\mathbb{I} - \lambda S \mathbf{H} + \mathbf{Q} \cdot \mathbf{H} - \mathbf{H} \cdot \mathbf{Q}$ where P is the pressure which

is fixed by the incompressibility condition. $\boldsymbol{\sigma}^E$ is the traceless Ericksen stress, see [35]. Finally, the molecular tensor $\mathbf{H} = -\delta F^{LDG}/\delta \mathbf{Q}$ where F^{LDG} is the Landau De-Gennes free energy given by

$$F^{LDG} = \frac{K}{2} \int [|\nabla \mathbf{Q}|^2 + \frac{1}{\epsilon^2} \text{tr} \mathbf{Q}^2 (\text{tr} \mathbf{Q}^2 - 1)] dA. \quad (3)$$

In the expression above, K denotes the single elastic constant and ϵ is a length scale which dictates the typical length scale over which S varies, often referred to as the defect core radius. We simulate the active nematic on a 512×512 periodic square grid to reach a steady state of defect chaos, see Fig. 1a,b and SI Movie 1. We set the length of the simulation area to be $L = 1$, the single elastic constant to be $K = 1$ which define our length and energy scales respectively. We set the rotational viscosity $\gamma = 1$ and re-scale time by $\tau = \gamma L^2 / K$; all results are given in re-scaled units. We set $\epsilon = 1.5/512$ which fixes the defect scale to be of the order of the grid spacing, and $\alpha = -0.125 \times 512^2$ which results in a simulation containing of the order of 10^2 defects reflecting typical experimental data sets [17]. We neglect flow alignment by setting $\lambda = 0$ and the viscosity is set to $\eta = 0.25$; we enforce low Reynolds number by simulating unsteady Stokes flow, setting $D_t \mathbf{v} = \partial_t \mathbf{v}$ [19]. Similar values have been shown to reproduce well the behaviour of microtubule based active nematics [17].

The total energy of an active nematic is the sum of the Landau De-Gennes free energy, F^{LDG} , and the kinetic energy given by $F^{KE} = \frac{1}{2} \int \rho v^2 dA$. Here we note that the Landau De-Gennes free energy is itself the sum of two components, $F^{LDG} = F^F + F^L$. F^F describes the energetic cost of variations in \mathbf{Q} ; in the nematic limit ($S = 1$) this becomes identical to the Frank free energy. F^L contains Landau terms governing the isotropic to nematic transition; this penalizes deviations of the scalar order parameter from $S = 1$. This is a key difference with previous work which was performed at the $S = 1$ limit, such that $F^L = 0$ [30, 32]. The contributions to the Landau De-Gennes free energy over Fourier space are plotted in Fig. 1c (here we use f^F and f^L to denote the energy densities associated with F^F and F^L , respectively). We observe a well defined peak in the elastic energy spectrum at wave number k^* . It has been shown that this peak is associated with the active length scale, $l_\alpha = \sqrt{K/|\alpha|}$ [30, 32]. We also see a clear exponential distribution of both f^F and f^L , indicating the existence of another length scale in the system; we confirm that this is related to the defect core radius, ϵ see [35].

When studying energy transfer, we consider the rate of change of total energy in the active nematic, namely $\dot{F} = \dot{F}_{KE} + \dot{F}_{LDG}$. This is a key distinction to previous works which consider only dissipation of kinetic energy in keeping with studies on classical turbulence [33, 34].

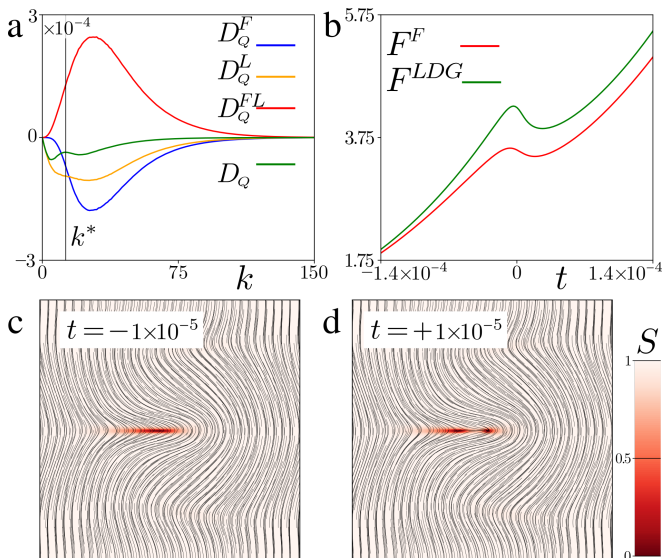


FIG. 2. (a) Spectra of the components of the rotational dissipation. The vertical line indicates the previously identified peak in energy injection, k^* . (b) Landau De-Gennes free energy (green) and distortion energy F^F (red) during defect nucleation via bend instability. The difference between the two lines shows the energy stored as deviations from $S = 1$. (c&d) Director field (lines) and scalar order parameter (color) immediately before (c) and after (d) defect creation via bend instability.

The change of total energy is calculated as:

$$\dot{F} = D_v + D_Q + T_{el} + I, \quad (4)$$

$$D_v = -2\eta \int u_{ij} u_{ij} \, dA, \quad (5)$$

$$D_Q = -\frac{1}{\gamma} \int H_{ij} H_{ij} \, dA, \quad (6)$$

$$T_{el} = - \int u_{ij} \sigma_{ij}^E \, dA, \quad (7)$$

$$I = -\alpha \int u_{ij} Q_{ij} \, dA. \quad (8)$$

Here we have used Einstein notation and repeated indexes are summed over. Respective contributions are identified as the energy dissipation due to shear viscosity, D_v , relaxation of the Q tensor, D_Q , the contribution from the Ericksen stress, T_{el} , and injection of energy due to active stresses, I , see [35] for a derivation.

When the system is at a steady state, such as that of fully developed defect chaos, there is no net gain or loss of energy, $\langle \dot{F} \rangle = 0$. However, when examining the various energy generation and dissipation terms in Fourier space, we observe a transfer between length scales, see Fig. 1d. The largest magnitude factors are active injection, I , and shear dissipation, D_v , which are peaked around a single length scale. This is in agreement with previous research which has identified the active length scale, l_α , as dominant during chaotic active nematic flows. The energy dissipation due to relaxation of the Ericksen stress

is the smallest magnitude term, and has little effect on energy transfer. However, the dissipation due to relaxation of Q has multiple peaks in magnitude, both above and below the peak of the injection and shear dissipation located at k^* . This leads to an energy transfer both up and down in length from that of active injection, shown as the black line in Fig. 1d. We also confirm that we do not observe any kinetic energy transfer between length scales, in agreement with previous studies [33, 34] and see Fig. S1[35].

The energy transfer between scales we observe is different from classical turbulence, for two key reasons. First, we are at low Reynolds number, and the convective term in the momentum equation is neglected. Second, we consider the sum of the kinetic and elastic energy of the fluid. Our results are also in disagreement with previous studies on energy transfer in active nematics which were performed at the $S = 1$ limit [30, 32]. Like in experiments, our simulations allow for variations in the scalar order parameter, which are penalized by the Landau terms in the free energy. We now examine how this modifies the dissipation due to relaxation of Q more closely. First, we can write D_Q as the sum of three terms

$$D_Q = D_Q^F + D_Q^L + D_Q^{FL} \quad (9)$$

$$D_Q^F = -\frac{K^2}{\gamma} \int [\partial_k^2 Q_{ij}] [\partial_t^2 Q_{ij}] \, dA \quad (10)$$

$$D_Q^L = -\frac{K^2}{2\gamma\epsilon^4} \int [S - S^3]^2 \, dA \quad (11)$$

$$D_Q^{FL} = -\frac{2K^2}{\gamma\epsilon^2} \int [1 - S^2] Q_{ij} \partial_k^2 Q_{ij} \, dA \quad (12)$$

D_Q^F describes energy dissipated by relaxing energy variations in Q , governed by f^F , and D_Q^L describes energy dissipated by relaxing deviations from $S = 1$, governed by f^L . Finally, D_Q^{FL} describes energy change due to exchange between f^F and f^L , see [35] for a derivation.

The contributions to D_Q are plotted in Fig. 2a. As expected, the relaxation terms D_Q^F and D_Q^L are both negative with a single peak. However, the energy lost relaxing gradients of Q and the order parameter, S , is offset in large part by an exchange between the two given by D_Q^{FL} which is positive. The combination of these factors leads to the multiple peaks observed in the magnitude of D_Q , which in turn leads to energy transfer. One of the primary mechanisms through which energy can be exchanged between f^F and f^L is the generation of topological defects; Fig. 2b shows the distribution of the elastic energy throughout this process. This happens when a constant Q field is no longer stable with respect to distortions in the orientation of the director due to the effect of active stress, which occurs at a critical wavelength that scales with the active length scale [19]. In an extensile active nematic, the bend deformation is unstable as shown in Fig. 2c. The deformation is penalized by the f^F term in the energy; this can be offset by reducing the order parameter from $S = 1$, which is in

turn penalized by the f^L terms in the energy; this leads to a co-localization of distortions in the director field with deviations from $S = 1$, see Fig. 2c. As the bend distortion grows, the local energy density increases until it becomes favorable to nucleate a pair of topological defects which results in a reduction in both forms of energy, see Fig. 2b. At this point, the bend distortion is replaced by a pair of topological defects and a splay distortion which is not unstable, see Fig. 2d. This process focuses all distortion in the director and the scalar order parameter into a small region localized around the topological defects.

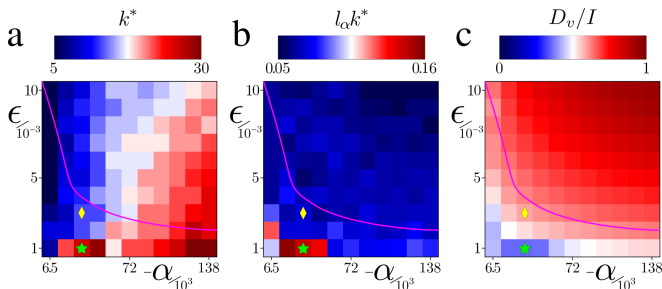


FIG. 3. (a) Peak of the energy transfer spectra as a function of activity, α , and defect core radius, ϵ . (b) Same as (a) with the waver number scaled by the active length scale. (c) Fraction of energy dissipated through viscosity as a function of activity, α , and defect core radius, ϵ . The yellow diamond indicates the location of simulations shown in Figs. 1,2. The green star shows the location of simulations shown in Fig. 4. The pink line indicates the ratio between defect density and defect size observed in experiments, see [35].

The active length, l_α , governs the length scale of many features of an active nematic and can be controlled by varying the activity, α . The other typically important length is the defect core radius, ϵ , which controls the balance between the two terms in the Landau De-Gennes free energy. Fig. 3a shows how the location of the positive peak in the energy transfer, k^* , varies with these two length scales. Almost all variation is with α , which we confirm by plotting $l_\alpha k^*$, see Fig. 3b. This confirms that in typical defect chaos, the key length scale governing energy transfer remains l_α . This is consistent with the earlier simulations, displayed as a yellow diamond, and microtubule based active nematic experiments, indicated by the pink line in Fig. 3b (see [35]). We also look at the dominant method of energy dissipation over the same parameter range. The total energy injection rate is given by I , which in turn is predominantly dissipated by viscosity through D_v and relaxation of the director D_Q . Thus D_v/I gives the fraction of energy dissipated through viscosity shown in Fig. 3c. Here we see that in typical defect chaos, the dominant method of energy dissipation is viscosity, consistent with previous numerical studies [32]. Defect chaos emerges when l_α is small, hence when activity, α , is high. High activity increases the flow speed, and thus strain rate, leading to an increase in D_v . Conversely, the relaxation of the director, D_Q , does not directly scale with the

activity thus during defect chaos D_v dominates energy dissipation; this is referred to as the high activity regime in numerical studies by Alert et al. [32]. However, we see that for small values of ϵ the scaling with l_α breaks down and the dominant method of dissipation is relaxation of Q , see Figs. 3b,c. When ϵ is very small, D_Q^L increases and eventually causes relaxation of the director, D_Q , to become the dominant method of energy dissipation, Fig. 3c. In this state, the Landau terms in the free energy dominate and the cost of topological defects becomes very high, furthermore when α is small the active length scale is large and less defects are expected. Thus we arrive at a state with a very low number of defects, see Fig. 4 and SI Movie 2.

The state identified in Fig. 4 occurs when ϵ is small and variations in the scalar order parameter from $S = 1$ are heavily penalized; this is reminiscent of recent numerical studies on active nematics in which the order parameter $S = 1$ is fixed and no energy transfer was observed [30, 32]. The dissipation spectra in this regime display a clear sign of energy transfer between length scales, see Fig. 4c. However, in contrast with defect chaos we see the emergence of a very strong energy sink due to D_Q at low wave number which becomes dominant. When we examine the individual contributions to D_Q we see that this additional dissipation is almost entirely due to relaxation of the scalar order parameter, D_Q^L , see Fig. 4d. As before, the peak in the elastic energy spectra occurs at the same wave number as the peak in active injection and shear dissipation, which is related to the active length scale, $k^* \sim l_\alpha^{-1}$. We see a small secondary peak in f^L at a similar wave number to the dominant energy sink, see Fig. 4e. Similar to the defective regime, we see an exponential distribution of energy at high wave numbers, see Fig. 4e (black dashed line), however we see the suggestion of an additional, longer length scale at lower wave numbers (red dashed line). We can visualize the structure of the energy associated with F^L by plotting the scalar order parameter, S , for the same simulation shown in Fig. 4a,b, see Fig. 4f. Here we see a clear structure of walls at which the order parameter $S < 1$; these walls arrange the space into long channels that correspond to the flow pattern shown in Fig. 4b.

To examine how this new state of active nematics arises, we look again at the change in elastic energy through a bend instability, see Fig. 4g. There is no longer a distinct drop in the energy as the system nucleates a pair of topological defects. In this regime, the cost of deviations from $S = 1$ are so high that rather than nucleating a pair of defects, the initial bend instability grows in length, resulting in a bend wall, see Fig. 4h. As before, the energy of this distortion can be reduced by locally decreasing S . However, since ϵ is small, this is associated with a high energetic cost. The result is a slight reduction of S in a narrow region where the distortions in the director can be focused into a bend wall, see Fig. 4h. These long bend walls focus the active stress resulting in a parallel laminar like flow, which leads

to reduced viscous dissipation, see Fig. 3c.

This new regime of active nematics features fewer defects but still exhibits energy transfer across length scales. Much like defect chaos, it arises specifically through the ability to exchange distortions in the director field with deviations from $S = 1$. It also has many interesting features that are not yet well understood. For example the bend walls have a tendency to form spirals. This is because when two bend walls wrap around each other they generate a rotating flow. In addition, defects move primarily along bend walls, releasing stored elastic energy rather than through self propulsion as in typical defect chaos [24]. Positive defects often appear at the end of a bend wall, generating an active flow which counteracts their motion back along the bend wall; this can result in positive defects becoming stalled. This new regime is visually similar to arrested flow patterns observed in numerical studies on active nematics at the $S = 1$ limit [37], with the key distinction that in our simulations the patterns remain highly dynamic, with constant reforming of defects and bend walls, see SI Movie 2.

In this manuscript we have demonstrated that energy transfer is expected across length scales in the defect chaos regime of active nematics, which is the state reported in the vast majority of experimental realizations. This comes primarily from the ability to exchange elastic energy between variations in the director field and the scalar order parameter, which are governed by the two components of the Landau De-Gennes free energy. We show that during defect chaos, energy is exchanged between these two forms through defect nucleation and annihilation, that the dominant length scale in this process is the active length scale, and that energy is predominantly dissipated through viscosity. We then identify a second regime in which the energetic cost of defect nucleation is greatly increased, leading to a new phase of active nematics that features extended dynamic bend walls, introducing additional large scale structures. These bend walls split the flow into laminar flow corridors which reduce viscous dissipation and can form self propagating spirals. These results deepen our understanding of fundamental, yet unsolved, features of active fluids that continue to fascinate us both in their similarities and differences with classical fluids.

ACKNOWLEDGMENTS

DJGP acknowledges funding from the Swiss National Science Foundation under starting grant TMSGI2 211367. J.I.-M., and F.S. acknowledge funding from MICIU/AEI/10.13039/501100011033 (Grant No. PID2022-137713NB-C21). The authors are indebted to the Brandeis University MRSEC Biosynthesis facility (supported by NSF MRSEC 2011846) for providing the tubulin to perform experiments. We thank Dom Corbett for insightful discussions.

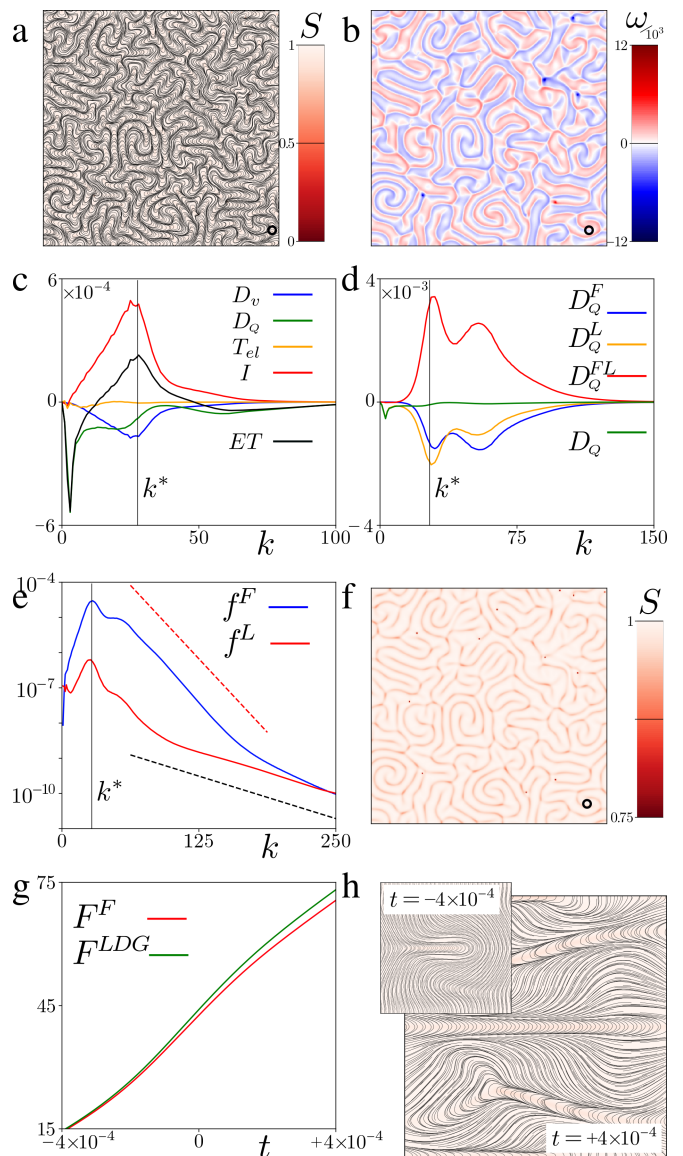


FIG. 4. (a&b) Director field and scalar order parameter (a) and vorticity (b) of a simulated active nematic in the regime where rotational dissipation dominates ($\alpha = -0.125 \times 512^2$, $\epsilon = 0.5/512$ indicated by the green star in Fig. 3b). The length scale associated with peak energy injection scale is indicated by the black circle in (a)&(b). (c) Dissipation spectra for a simulated active nematic in the rotational dissipation regime. There is a dominant energy sink at small wave numbers. (d) Spectra of the components of the rotational dissipation in this regime. (e) Spectra for the Landau De-Gennes free energy showing the distortion (blue) and order (red) separately for the rotational dissipation regime. The black dashed line shows a similar exponential as in Fig. 1c rescaled for the reduced value of ϵ . The red dashed line shows the emergence of a second, longer length scale; see [35] for details. (f) Scalar order parameter for simulated active nematic in the rotational dissipation regime (same simulation as (a)&(b)). (g) Energy density of the different components of the Landau De-Gennes free energy during bend instability. Time $t = 0$ is defined at the point at which the bend wall completely spans the periodic boundaries and the previously identified nucleation process is ruled out. (h) Bend instability leads to the generation of bend walls which extend over the system size. All results in this figure are simulated in the rotational dissipation regime with $\alpha = -0.125 \times 512^2$, $\epsilon = 0.5/512$.

-
- [1] S. Ramaswamy, The mechanics and statistics of active matter, *Annu. Rev. Condens. Matter Phys.* **1**, 323 (2010).
- [2] S. Ramaswamy, Active matter, *Journal of Statistical Mechanics: Theory and Experiment* **2017**, 054002 (2017).
- [3] M. C. Marchetti, J.-F. Joanny, S. Ramaswamy, T. B. Liverpool, J. Prost, M. Rao, and R. A. Simha, Hydrodynamics of soft active matter, *Reviews of modern physics* **85**, 1143 (2013).
- [4] F. Sagués, *Colloidal Active Matter* (Taylor and Francis Group, Boca Raton, FL, 2023).
- [5] D. J. Pearce, L. Hoogerbrugge, K. A. Hook, H. S. Fisher, and L. Giomi, Cellular geometry controls the efficiency of motile sperm aggregates, *Journal of the Royal Society Interface* **15**, 20180702 (2018).
- [6] S. F. Schoeller, W. V. Holt, and E. E. Keaveny, Collective dynamics of sperm cells, *Philosophical Transactions of the Royal Society B* **375**, 20190384 (2020).
- [7] N. C. Makris, P. Ratilal, S. Jagannathan, Z. Gong, M. Andrews, I. Bertatos, O. R. Godø, R. W. Nero, and J. M. Jech, Critical population density triggers rapid formation of vast oceanic fish shoals, *Science* **323**, 1734 (2009).
- [8] A. Doostmohammadi, J. Ignés-Mullol, J. M. Yeomans, and F. Sagués, Active nematics, *Nature communications* **9**, 3246 (2018).
- [9] F. Juelicher, K. Kruse, J. Prost, and J.-F. Joanny, Active behavior of the cytoskeleton, *Physics reports* **449**, 3 (2007).
- [10] L. Balasubramaniam, R.-M. Mège, and B. Ladoux, Active nematics across scales from cytoskeleton organization to tissue morphogenesis, *Current Opinion in Genetics & Development* **73**, 101897 (2022).
- [11] T. B. Saw, W. Xi, B. Ladoux, and C. T. Lim, Biological tissues as active nematic liquid crystals, *Advanced materials* **30**, 1802579 (2018).
- [12] R. Mueller, J. M. Yeomans, and A. Doostmohammadi, Emergence of active nematic behavior in monolayers of isotropic cells, *Physical review letters* **122**, 048004 (2019).
- [13] V. Yashunsky, D. J. Pearce, G. Ariel, and A. Be'er, Topological defects in multi-layered swarming bacteria, *Soft Matter* **20**, 4237 (2024).
- [14] Z. You, D. J. Pearce, A. Sengupta, and L. Giomi, Geometry and mechanics of microdomains in growing bacterial colonies, *Physical Review X* **8**, 031065 (2018).
- [15] T. Sanchez, D. T. Chen, S. J. DeCamp, M. Heymann, and Z. Dogic, Spontaneous motion in hierarchically assembled active matter, *Nature* **491**, 431 (2012).
- [16] P. Guillamat, Ž. Kos, J. Hardoüin, J. Ignés-Mullol, M. Ravník, and F. Sagués, Active nematic emulsions, *Science advances* **4**, eaao1470 (2018).
- [17] D. Pearce, J. Nambisan, P. Ellis, A. Fernandez-Nieves, and L. Giomi, Orientational correlations in active and passive nematic defects, *Physical Review Letters* **127**, 197801 (2021).
- [18] S. J. DeCamp, G. S. Redner, A. Baskaran, M. F. Hagan, and Z. Dogic, Orientational order of motile defects in active nematics, *Nature materials* **14**, 1110 (2015).
- [19] L. Giomi, Geometry and topology of turbulence in active nematics, *Physical Review X* **5**, 031003 (2015).
- [20] D. J. Pearce and K. Kruse, Properties of twisted topological defects in 2d nematic liquid crystals, *Soft Matter* **17**, 7408 (2021).
- [21] X. Tang and J. V. Selinger, Orientation of topological defects in 2d nematic liquid crystals, *Soft matter* **13**, 5481 (2017).
- [22] A. J. Vromans and L. Giomi, Orientational properties of nematic disclinations, *Soft matter* **12**, 6490 (2016).
- [23] S. P. Thampi, R. Golestanian, and J. M. Yeomans, Instabilities and topological defects in active nematics, *Europhysics Letters* **105**, 18001 (2014).
- [24] L. Giomi, M. J. Bowick, P. Mishra, R. Sknepnek, and M. Cristina Marchetti, Defect dynamics in active nematics, *Philosophical Transactions of the Royal Society A: Mathematical, Physical and Engineering Sciences* **372**, 20130365 (2014).
- [25] P. K. Kundu, I. M. Cohen, and D. R. Dowling, *Fluid mechanics* (Academic press, 2015).
- [26] C.-M. Koch and M. Wilczek, Role of advective inertia in active nematic turbulence, *Physical Review Letters* **127**, 268005 (2021).
- [27] A. Opatthalage, M. M. Norton, M. P. Juniper, B. Langeslay, S. A. Aghvami, S. Fraden, and Z. Dogic, Self-organized dynamics and the transition to turbulence of confined active nematics, *Proceedings of the National Academy of Sciences* **116**, 4788 (2019).
- [28] A. Doostmohammadi, T. N. Shendruk, K. Thijssen, and J. M. Yeomans, Onset of meso-scale turbulence in active nematics, *Nature communications* **8**, 15326 (2017).
- [29] P. Guillamat, J. Ignés-Mullol, and F. Sagués, Taming active turbulence with patterned soft interfaces, *Nature Communications* **8**, 564 (2017), 1611.06416.
- [30] R. Alert, J.-F. Joanny, and J. Casademunt, Universal scaling of active nematic turbulence, *Nature Physics* **16**, 682 (2020).
- [31] B. Martínez-Prat, R. Alert, F. Meng, J. Ignés-Mullol, J.-F. Joanny, J. Casademunt, R. Golestanian, and F. Sagués, Scaling regimes of active turbulence with external dissipation, *Physical Review X* **11**, 031065 (2021).
- [32] R. Alert, J. Casademunt, and J.-F. Joanny, Active turbulence, *Annual Review of Condensed Matter Physics* **13**, 143 (2022).
- [33] J. Urzay, A. Doostmohammadi, and J. M. Yeomans, Multi-scale statistics of turbulence motorized by active matter, *Journal of Fluid Mechanics* **822**, 762 (2017).
- [34] L. N. Carenza, L. Biferale, and G. Gonnella, Cascade or not cascade? energy transfer and elastic effects in active nematics, *Europhysics Letters* **132**, 44003 (2020).
- [35] Supplementary material, [URL_will_be_inserted_by_publisher](#).
- [36] A. N. Beris and B. J. Edwards, *Thermodynamics of Flowing Systems: with Internal Microstructure* (Oxford Science Publications, 1994).
- [37] I. Lavi, R. Alert, J.-F. Joanny, and J. Casademunt, Dynamical arrest in active nematic turbulence, arXiv preprint arXiv:2407.15149 (2024).